We are IntechOpen,
the world's leading publisher of
Open Access books
Built by scientists, for scientists

4,800
Open access books available

122,000
International authors and editors

135M
Downloads

Our authors are among the

154
Countries delivered to

TOP 1%
most cited scientists

12.2%
Contributors from top 500 universities

CLARIVATE ANALYTICS
BOOK CITATION INDEX
INDEXED

WEB OF SCIENCE™

Selection of our books indexed in the Book Citation Index
in Web of Science™ Core Collection (BKCI)

Interested in publishing with us?
Contact book.department@intechopen.com

Numbers displayed above are based on latest data collected.
For more information visit www.intechopen.com

Chapter

Clustering Techniques for Land Use Land Cover Classification of Remotely Sensed Images

Debasish Chakraborty

Abstract

Image processing is growing fast and persistently. The idea of remotely sensed image clustering is to categorize the image into meaningful land use land cover classes with respect to a particular application. Image clustering is a technique to group an image into units or categories that are homogeneous with respect to one or more characteristics. There are many algorithms and techniques that have been developed to solve image clustering problems, though, none of the method is a general solution. This chapter will highlight the various clustering techniques that bring together the current development on clustering and explores the potentiality of those techniques in extracting earth surface features information from high spatial resolution remotely sensed imageries. It also will provide an insight about the existing mathematical methods and its application to image clustering. Special emphasis will be given on Hölder exponent (HE) and Variance (VAR). HE and VAR are well-established techniques for texture analysis. This chapter will highlight about the Hölder exponent and variance-based clustering method for classifying land use/land cover in high spatial resolution remotely sensed images.

Keywords: remote sensing image, clustering, classification, land use, land cover, features, extraction

1. Introduction

High spatial resolution remotely sensed imagery helps to obtain quality and detailed information about the earth's surface features in conjunction with their geographical associations. The internal changeability within the identical land-use land-cover units augments with the rise of resolution. The augmented changeability diminishes the statistical distinguishability of land-use/land-cover classes in the spectral data space. This reduced distinguishability tends to decrease the accuracies of pixel-based clustering algorithms such as Fuzzy C Means [1], minimum distance classifiers [2] and K-Means [3]. These pixel-based clustering techniques assign a pixel to a region according to the similarities of spectral signature. It considers only one pixel at a time [4]. Spectral signatures are the specific combination of emitted, reflected or absorbed electromagnetic (EM) radiation at varying wavelengths which can uniquely identify an object [4].

Compared to IRS-1A/1B sensors, the spectral resolution of high spatial resolution images is normally relatively poor. Spectral resolution describes a sensor's ability to

identify fine intervals of wavelength. The better the spectral resolution, the finer the channel or band width. Therefore, between spatial and spectral resolution, there is a trade-off. It is mainly true for panchromatic (PAN) images of high spatial resolution, namely CARTOSAT-II 1m and IKONOS 1m. There is a need to consider the spatial relationships between pixel values, also known as the 'texture' of the scene objects to classify high-resolution (HR) images owing to the wide difference in the spatial structure in these images. Consequently, multiple texture-based clustering technique namely GLCM [5–8], Markov random field (MRF) model [5], Gray scale rotation invariant [9] were evolved for clustering remote sensing images having high spatial resolution. Nevertheless, above mentioned methods are appropriate in textured area of HR images. A region is called textured; where the intensity dissimilarity within adjacent pixels is substantial. A region is said to be non-textured, where the intensity dissimilarity among adjacent pixels is insignificant [10, 11]. But texture-based classification techniques failed in non-textured region of high spatial resolution image as much variation is not found in the spatial pattern of those regions of the image [12]. Thus, we can infer from earlier studies that classification of high spatial resolution imageries either by pixel or texture-based algorithm may not yield desired results.

Some more techniques namely watershed approach [13, 14], region-growing approach [4, 15], mean shift approach [16, 17], region merging approach [18] etc. are in use for clustering high spatial resolution remote sensing images. Application of these approaches for clustering of images either leads to under-segmentation or over-segmentation [19, 20]. Structural image indexing approach [21], semi-supervised feature learning approach [22] and multi-scale manner using SVM approach [23] are also found fairly suitable in clustering high resolution images. The imagery of higher resolution includes textured and non-textured areas. Hence, pixel or texture-based algorithm for clustering of high-resolution imagery does not produce expected results. This type of high-resolution imagery clustering research is in the trend. Multi-circular local binary pattern and variance-based method [10] were used separately to cluster high resolution image having textured and non-textured regions. The Multi circular local binary pattern operator has been used here for measuring the spatial structure of the image. But, disadvantage in this strategy is that multi-circular local binary pattern operator is susceptible to noise as it exactly sees the value of the moving window's central pixel as a limit for computing the spatial structure around the central pixel.

In last one decade the Hölder exponent (HE) has been used for calculating spatial structure of the images [24–26]. It is also being used for clustering high-resolution images [12]. HE gives an evidence of the spatial structure of the image and is not much influenced by the noise. In addition, spatial structure, contrast of the local image holds considerable property for calculating the texture around the pixel. In this research, high-resolution picture textured and non-textured region is originally segmented using HE and VAR-based method and subsequently separately clustered and non-textured areas. VAR is used to calculate the contrast around the pixel. The suggested method is applied with a 1 m spatial resolution on high resolution IKONOS PAN images.

2. Methods

The suggested high-resolution image 'P' clustering technique has three main steps: (i) image transformation, (ii) segmentation and extraction, and (iii) clustering. Initially, every pixel of the image is converted into a degree of texture or non-texture around the pixel. In the second step, using segmented image mask, the transformed

image is segmented and non-textured and textured regions are extracted from the initial image. Finally, the two areas obtained are separately clustered.

2.1 Transformation of image

The Hölder Exponent (HE) and VAR are jointly used to convert the image for computing the texture. The HE calculates each pixel of P's spatial structure. Besides spatial structure, local image contrast also grasps important property for computing the texture around the pixel. In this research, therefore, VAR is used to calculate the contrast around the pixel.

2.1.1 Hölder exponent

Hölder exponent has been used for investigating the texture in high-resolution images [12]. It measures the irregularity in the vicinity. Supremacy of applying Hölder Exponent in HR images are that (i) it can be used as an instrument to calculate each pixel of the image's spatial structure, (ii) no previous data on the pixel intensity is required and (iii) is not very sensitive to noise [12].

Definition of HE [27]: Let μ be a measure on a set Ω as well as for all $x \in \Omega$, $\ni \alpha(x)$, such that $\mu(B_r(x)) \sim r^\alpha$, for small r. Here $B_r(x)$ is circle (2D) of radius i centered on x. Then $\alpha(x)$ is called the HE on x.

A sequence of 15 values of radius r (i.e. $1, \sqrt{2}, \sqrt{5}, 3, \sqrt{13}, 3\sqrt{2}, 5, \sqrt{29}, 2\sqrt{10}, 3\sqrt{5}, 7, \sqrt{61}, 6\sqrt{2}, \sqrt{85}, 7\sqrt{2}$) centered on x are used as a scale parameter for calculating HE value around each pixel x in the image [12] and the total number (N) of intersected pixels by the perimeter of series of circles of radius r is considered as a scale parameter for computing VAR value around x [12]. N is computed using Eq. (1).

$$N = \sum_{r=1}^{t} m_r \tag{1}$$

where t is the total number of identified circles, m_r is the number of intersected pixels on the perimeter of the radius r circle.

2.1.2 VAR (σ^2) for contrast measurement around each pixel of the image

To get the contrast value of (x, y), the neighbor's σ^2 of each pixel (x, y) is calculated over the entire image. Using Eq. (2), the σ^2 (x, y) is realized

$$\sigma^2(x,y) = \frac{\sum_{r=1}^{t}\sum_{j=1}^{m_r}(a_{rj} - \mu)^2}{N} \tag{2}$$

where a_{rj} is the intensity value of pixel (r,j),

$$\mu = \frac{\sum_{r=1}^{t}\sum_{j=1}^{m_r} a_{rj}}{N}$$

Thus obtained $\alpha(x,y)$ and σ^2 (x,y) for each P(x,y). Afterward, these values are used in Eq. (3) to obtain the corresponding pixel value (x,y) in the transformed image T. Each pixel (x,y) of T signifies the degree of texture around that pixel.

$$T(x,y) = \frac{\alpha(x,y) + \sigma^2(x,y)}{2} \tag{3}$$

2.2 Image segmentation and extraction

The image 'T' is segmented into textured and non-textured regions based on a threshold value 'δ'. The pixel value in T below the 'δ' is considered to be a non-textured region, whereas greater than or equal to 'δ' is considered to be the textured region in the segmented image. Pixels are labeled as zero in non-textured areas, whereas pixels are marked as one in textured areas in the segmented image mask and depicted as follows:

$$\Gamma(x, y) = \begin{cases} 1, T(x,y) \geq \delta \\ 0, T(x,y) < \delta \end{cases} \tag{4}$$

where T(x,y) and Γ(x,y) represents the pixel value in (x,y) position of the two dimensional transformed image and segmented image respectively and δ represents the threshold value. The δ is calculated by using Eq. (5).

$$\delta = T_{min} + \frac{T_{max} - T_{min}}{K} \tag{5}$$

where T_{min} and T_{max} represents minimum and maximum pixel gray value in T respectively and K is user defined value.

IKONOS PAN sensor image of size 256×256 pixels (shown in **Figure 1a**) is used to achieve the optimum K. The suggested clustering method is also implemented for distinct K values on this image.

The segmented image is subsequently used to obtain the textured and non-textured region from the initial image P. This process's mathematical representation is shown as follows:

$$R_1(x, y) = \begin{cases} P(x, y), & \Gamma(x, y) = 0 \\ 0, & \Gamma(x, y) \neq 0 \end{cases} \tag{6}$$

$$R_2(x, y) = \begin{cases} P(x, y), & \Gamma(x, y) = 1 \\ 0, & \Gamma(x, y) \neq 1 \end{cases} \tag{7}$$

where P, Γ, R_1 and R_2 indicates original image, segmented image, extracted non-textured region from original image P and extracted textured region from original image P respectively.

2.3 Clustering

Initially, a threshold is used to segment the transformed image into textured and non-textured region. Afterward, the original image is extracted into textured and non-textured regions using the segmented image mask and clustered independently. The extracted textured region (R_2) is clustered by means of ISODATA clustering algorithm [28] considering HE, VAR and intensity values of individual pixel of textured area. The clustering algorithm of ISODATA is less computational, easy and non-supervisory. Whereas the non-textured area (R1) of the image is categorized using the clustering algorithm of ISODATA. In the event of non-textured region, the individual pixel HE and VAR value is not regarded for classification as there is no important variation in texture between classes. The classified outputs of the non-textured and textured region are subsequently produced separately and mixed together to obtain the final classified image.
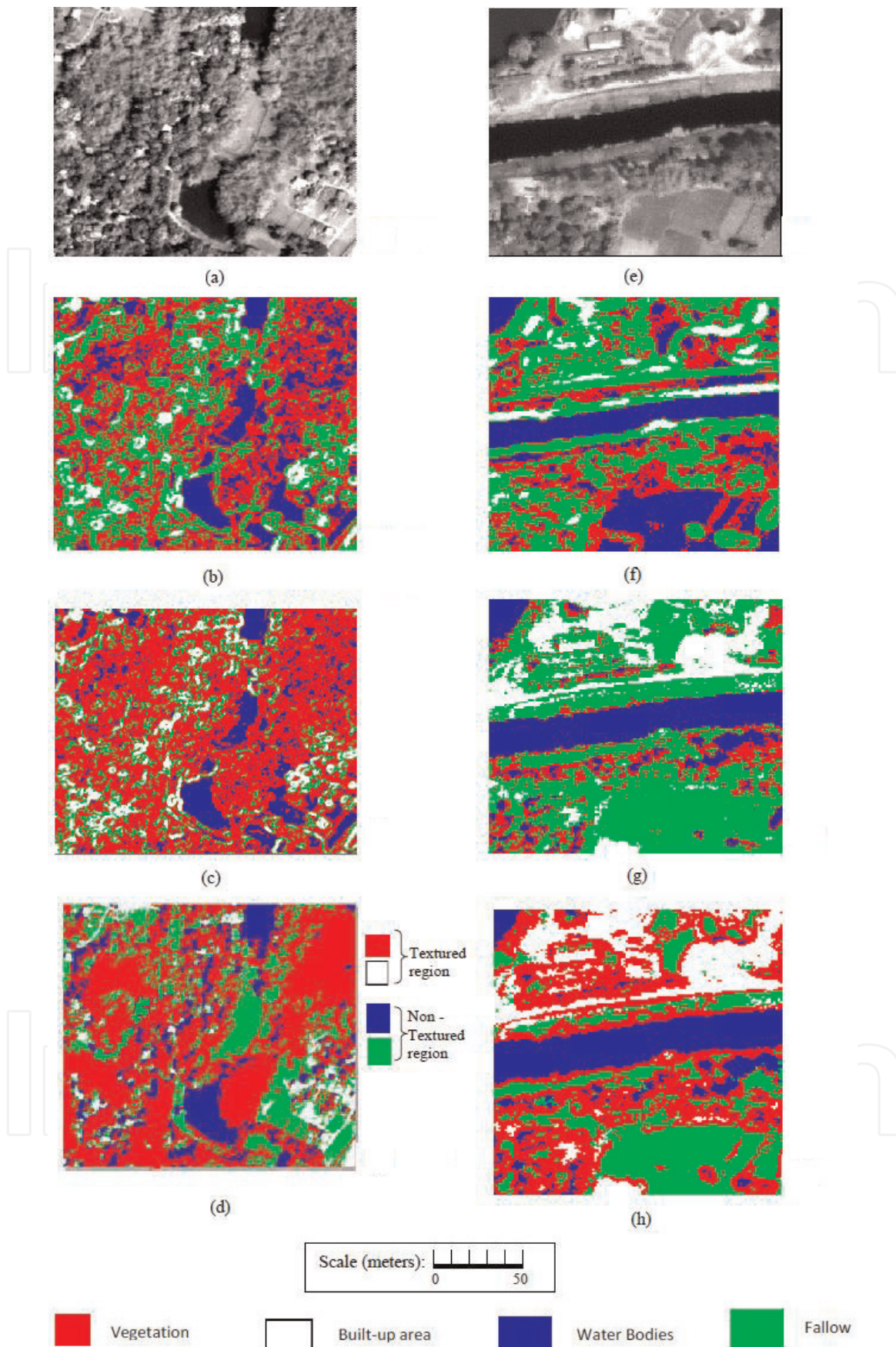
Figure 1.
*(a) IKONOS image showing vegetation, built-up area, fallow and water body categories, (b) classified image obtained by applying "HE-VAR and PAN" based method on **Figure 1a**, (c) classified image obtained by applying "MCLBP and VAR" based method on **Figure 1a**, (d) classified image obtained by applying "proposed classification method" on **Figure 1a**, (e) IKONOS image showing fallow, water bodies, vegetation and built-up area categories, (f) classified image obtained by applying "HE-VAR and PAN" based method on **Figure 1e**, (g) classified images obtained by applying "MCLBP and VAR" based method on **Figure 1e**, (h) Classified images obtained by applying "proposed classification method" on **Figure 1e**.*

This research uses "HE-VAR and PAN" and "MCLBP and VAR" based clustering technique to show the power of the suggested clustering technique. The technique based on "HE-VAR and PAN" clusters the entire image using the HE, VAR and intensity of each pixel of the IKONOS PAN image. The suggested technique of clustering is then contrasted with the outcomes of the clustering method based on "HE-VAR and PAN" and "MCLBP and VAR" to demonstrate the strength of the suggested technique of clustering.

3. Results and discussion

The projected clustering method imagines threshold δ to get the segmented image mask from the transformed image. The threshold is computed using a constant 'K'. In this study, proposed clustering procedure is implemented on IKONOS PAN image with spatial resolution 1 m for 'K' values between 3 and 7 and subsequently, classification rate is measured for these 'K' values using the ground truth data. The classification accuracy with different 'K' is shown in **Figure 2**. The 'K' affects the accuracy in classifying High spatial resolution images considerably as shown in **Figure 2**. For computing texture, a suitable choice of 'K' is important. In this study, superlative performance in high-resolution image classification was accomplished with K = 5. The optimum K is discovered based on **Figure 1a** and is also implemented in the classification of **Figure 1e** in addition to other images and found classification accuracy is more than 88%. Thus, from the present study, we can infer that the same K value is suitable for most images.

The Proposed clustering method, "MCLBP and VAR" based method and "HE-VAR and PAN" based method were applied on two different 1 m PAN (IKONOS) images (size 256 × 256 pixels) covering (i) vegetation, (ii) built-up area, (iii) water bodies, and (iv) fallow (shown in **Figure 1a, e**). Texture is observable in in **Figure 1a, e**. The results of proposed method are then compared with the results obtained from the analysis based on "HE-VAR and PAN" and "MCLBP and VAR" respectively.

Figure 1f–h shows the classification outcomes of the methods "HE-VAR and PAN," "MCLBP and VAR" and "Proposed classification" after proceeding to the second IKONOS image respectively. **Figure 1b–d** shows the classification outcomes of the methods "HE-VAR and PAN," "MCLBP and VAR" and "Proposed classification" after proceeding to the first IKONOS image respectively. Classified images recognize varied features in **Figure 1b–d, f–h**. From the results, it is evident that the
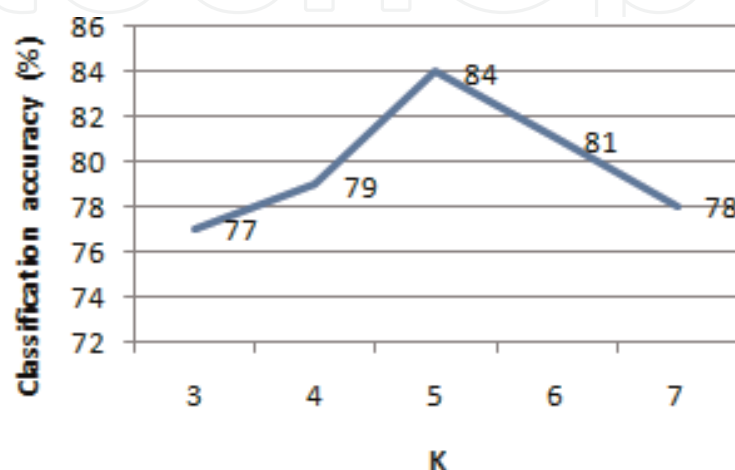

Figure 2.
Classification accuracy as a function of K.

method based on "MCLBP and VAR" gives less heterogeneous segments than the method based on "HE-VAR and PAN," while the method based on "Proposed classification method" provides more homogeneous segments with distinct classes than the method based on "MCLBP and VAR."

The ground truth data is collected using GPS equipment for the class vegetation, built-up area, fallow and water body of sample size of 656, 519, 577 and 462 square meters respectively. Afterward, ArcGIS software is used to transfer the ground truth data into vector data. Subsequently, by overlaying the ground truth information distinctly on the results acquired from both IKONOS images (**Figure 1a, e**) adopting methods such as "HE-VAR and PAN," "MCLBP and VAR" and "Proposed clustering," the classification accuracies for each strategy are shown by confusion matrix. The confusion matrices (**Table 1**) calculated for **Figure 1b–d** showed that the precision of classification of vegetation, built-up area, fallow and water bodies is (73, 69, 59 and 87% respectively) based on the 'HE-VAR and PAN' technique and (79, 71, 68 and 89% respectively) based on the 'MCLBP and VAR 'technique, whereas (91, 86, 85 and 94% respectively) by the "Proposed clustering" method. **Table 2** demonstrates the confusion matrices calculated for **Figure 1f–h** showed that the precision of classification of vegetation, built-up area, fallow and water bodies is (73, 74, 66 and 88% respectively) based on the 'HE-VAR and PAN 'technique and (78, 76, 68 and 89% respectively) based on the 'MCLBP and VAR 'technique whereas (90, 87, 86 and 93% respectively) by the "Proposed clustering" method.

The categorized result for **Figure 1a, e** shows that the "HE-VAR and PAN" method under segment as a result (i) fallow assorted with water bodies shown in **Figure 1b, f**, (ii) built-up region assorted with fallow and vegetation shown in **Figure 1f**, (iii) vegetation assorted with water bodies shown in **Figure 1b, f**, (iv) fallow assorted with built-up region shown in **Figure 1b**. This incoherence decreases vegetation, fallow, water bodies and built-up area classification precision as shown in **Tables 1** and **2**. The technique based on "MCLBP and VAR" somehow overcomes these inconsistencies. It is discovered that, as shown in **Figure 1c, g**, the superposition of fallow, water body, vegetation region becomes less. In addition, decreased inconsistencies improve the accuracy of the classification of fallow, water body and vegetation regions (see **Tables 1** and **2**).

"HE-VAR and PAN" based method classifies water bodies and fallow areas as a single class (**Figure 1b, f**) since the texture patterns of these two areas does not show much difference in high resolution imageries as shown in **Figure 1a, e**. "MCLBP and VAR" based technique demonstrates improvement in classifying the fallow areas and water bodies which is observable in **Figure 1g**. But this method could not extract non-textured region appropriately form **Figure 1a** since MCLBP is sensitive to noise. Therefore "MCLBP and VAR" based method could not discriminate appropriately fallow areas and water bodies in **Figure 1a** as visible in **Figure 1c**. HE is not as much of sensitive to noise therefore the proposed technique partitions the image into textured and non-textured regions noticeably which in turn helps in classifying the fallow and water bodies as shown in **Figure 1d**.

The proposed clustering method is applied further on a 1 m PAN (IKONOS) image (**Figure 3a**) of (i) urban woodland, (ii) building, (iii) water bodies, and (iv) fallow to show the robustness and validity of the method in classifying land use area. The method satisfactorily discriminate urban woodland, building, fallow and water bodies as shown in **Figure 3b**. The algorithm also implemented on two extra 1 m PAN (IKONOS) images: (i) **Figure 4a** of fallow, vegetation, built-up area and bare land and (ii) **Figure 4c** of water, vegetation, fallow and built-up area. The findings (**Figure 4b, d**) show that vegetation, fallow, built-up region, bare soil and water bodies are satisfactorily discriminated against by the algorithm.

		Classes derived from satellites							
Classification method	**Grand observed class**	**Vegetation**	**Built-up area**	**Fallow**	**Water body**	Row total	**Classification accuracy (%)**	**C (%)**	**O (%)**
HE-VAR and PAN	Vegetation	251	35	12	7	305	72.75	27.24	15.65
	Built-up area	18	163	14	5	200	69.07	30.93	15.68
	Fallow	53	23	144	14	234	59.26	40.74	37.04
	Water body	23	15	73	177	288	87.19	12.81	54.67
	Column total	345	236	243	203	1027			
MCLBP and VAR	Vegetation	272	31	11	4	332	78.84	18.26	13.33
	Built-up area	17	168	7	3	205	71.25	28.81	11.41
	Fallow	43	21	166	15	223	68.33	31.69	32.51
	Water body	13	16	59	181	258	89.28	10.83	43.35
	Column total	345	236	243	203	1027			
Proposed method	Vegetation	313	17	7	3	340	90.85	9.27	7.82
	Built-up area	7	204	8	2	221	86.28	13.56	7.20
	Fallow	19	7	206	7	239	84.77	15.23	13.58
	Water body	6	8	22	191	227	94.11	5.91	17.73
	Column total	345	236	243	203	1027			

C: Commission error, O: Omission error.

Table 1.
The confusion matrices showing the classification accuracy obtained by applying "HE-VAR and PAN", "MCLBP and VAR" and "Proposed" methods separately on IKONOS image shown in **Figure 1a**.

Classification method	Grand observed class	Classes derived from satellites					Classification accuracy (%)	C (%)	O (%)
		Vegetation	Built-up area	Fallow	Water body	Row total			
HE-VAR and PAN	Vegetation	228	15	43	16	302	73.3	26.68	23.79
	Built-up area	32	209	14	5	260	73.7	26.14	18.02
	Fallow	27	27	221	11	286	66.3	33.83	19.46
	Water body	24	32	56	227	339	87.6	12.35	43.24
	Column total	311	283	334	259	1187			
MCLBP and VAR	Vegetation	241	13	38	9	301	77.6	22.51	20.58
	Built-up area	29	215	13	7	264	75.83	24.02	17.31
	Fallow	26	26	228	11	291	68.36	31.74	18.86
	Water body	15	29	55	232	331	89.4	10.42	38.22
	Column total	311	283	334	259	1187			
Proposed method	Vegetation	281	7	14	6	308	90.4	9.64	8.68
	Built-up area	3	244	9	5	261	86.7	13.78	6.0
	Fallow	15	15	287	7	324	85.8	14.07	11.07
	Water body	12	17	24	241	294	93.2	6.94	20.46
	Column total	311	283	334	259	1187			

C: Commission error, O: Omission error.

Table 2.
The confusion matrices showing the classification accuracy obtained by applying "HE-VAR and PAN", "MCLBP and VAR" and "Proposed" methods separately on IKONOS image shown in **Figure 1e**.
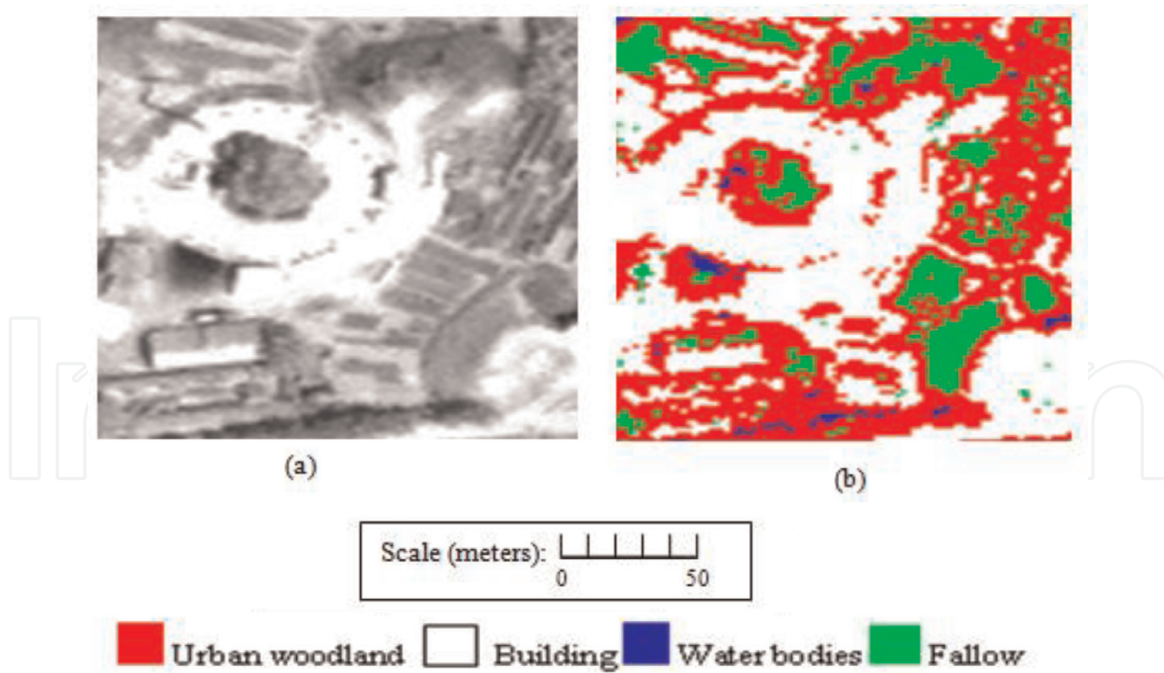
Figure 3.
(a) IKONOS image showing urban woodland, building, water body and fallow categories, (b) classified image obtained by applying "proposed classification method" on **Figure 3a***.*
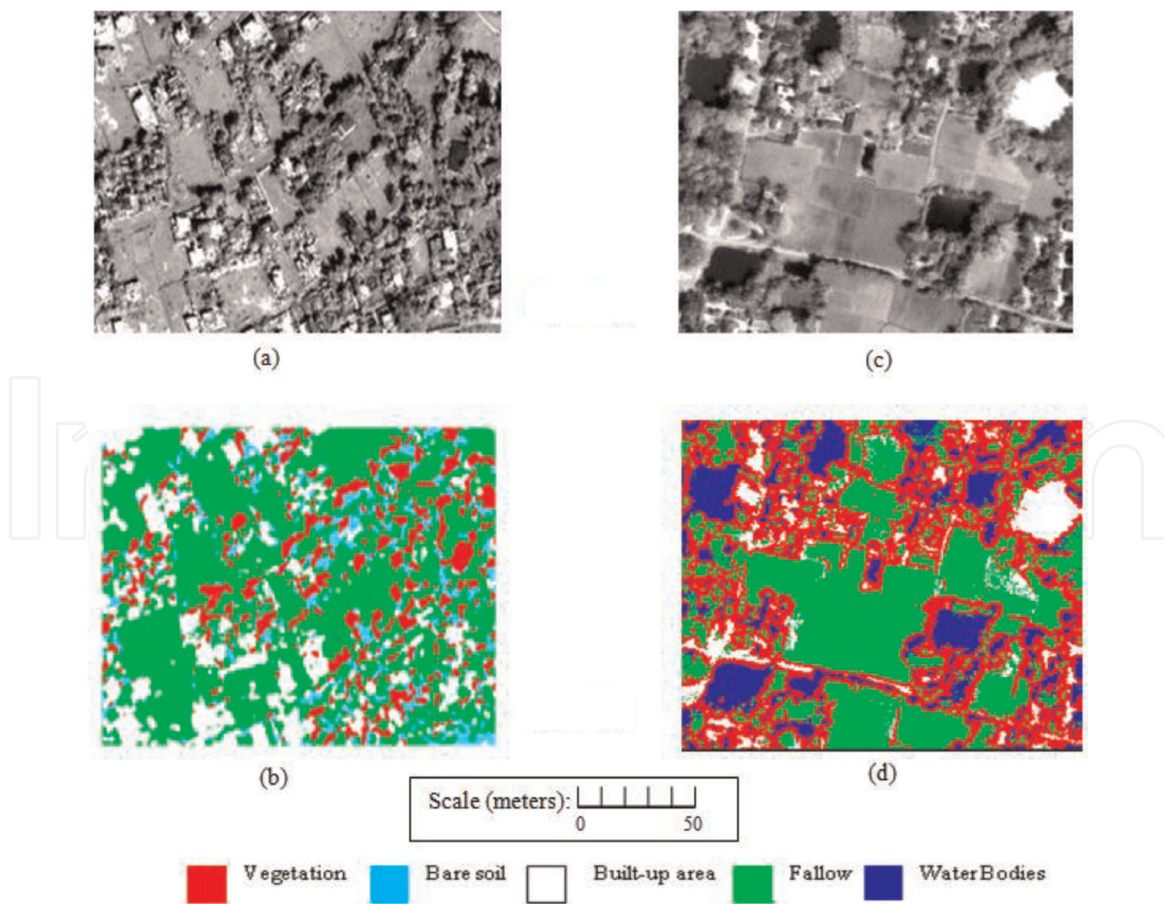

Figure 4.
(a) IKONOS image showing fallow, built-up area, vegetation and bare soil categories, (b) classified image obtained by applying "proposed classification method" on **Figure 4a***, (c) IKONOS image showing vegetation, fallow, built-up area and water bodies categories, (d) classified image obtained by applying "proposed classification method" on* **Figure 4c***.*

4. Conclusion

In the present study, the spatial structure of local image texture is computed using HE. The contrast around the pixel is measured using VAR. Afterward, the image is transformed using HE and VAR together for measuring the texture. A threshold δ is used to extract textured and non-textured region from the image. The classification algorithm ISODATA is used to classify the textured region taking into account HE, VAR and intensity values of the textured area's individual pixels. Whereas ISODATA clustering algorithm classifies the extracted non-textured region of the image. The HE and VAR value of individual pixels is not regarded for classification in the event of non-textured region. From the research outcomes, it is discovered that the suggested technique is helpful to extract earth surface characteristics from complicated remote sensing images that contain both textured and non-textured areas. Moreover, it can be considered as an intuitively appealing and unsupervised clustering algorithm for extracting features from remotely sensed images. As a result, the method is potentially useful to extract earth surface features by clustering high spatial resolution panchromatic images more efficiently.

Acknowledgements

Author details

Debasish Chakraborty
Regional Remote Sensing Centre-East, National Remote Sensing Centre, ISRO, New Town, Kolkata, West Bengal, India

*Address all correspondence to: deba.isro@gmail.com

IntechOpen

References

[1] Bezdek JC, Ehrlich R, Full W. FCM: The Fuzzy C-Means clustering algorithm. Computers and Geosciences. 1984;**10**:191-203

[2] Richards JA. Remote Sensing Digital Image Analysis: An Introduction. Berlin, Heidelberg: Springer-Verlag; 1995. pp. 265-290

[3] Hartigan JA, Wong MA. A K-means clustering algorithm. Applied Statistics. 1979;**28**(1):100-108

[4] Chakraborty D, Sen GK, Hazra S. Image Segmentation Techniques. Germany: LAP LAMBERT Academic Publishing; 2012. pp. 1-128

[5] Clausi DA, Yue B. Texture segmentation comparison using grey level co-occurrence probabilities and Markov random fields. In: Proceedings of the 17th International Conference on Pattern Recognition (ICPR'04); 2004. Available from: http://ieeexplore.ieee.org/stamp/

[6] Haralick RM, Shanmugan K, Dinstein I. Textural features for image classification. IEEE Transactions on Systems, Man, and Cybernetics. 1973;**6**:610-621

[7] Tsai F, Chou MJ. Texture augmented analysis of high resolution satellite imagery in detecting invasive plant species. Journal of the Chinese Institute of Engineers. 2006;**29**(4):581-592

[8] Tsai F, Chou MJ, Wang HH. Texture analysis of high resolution satellite imagery for mapping invasive plants. In: International Geoscience and Remote Sensing Symposium; 2005. pp. 43024-43027

[9] Klemas VV. Remote sensing of coastal resources and environment. Environmental Research, Engineering and Management. 2009;**2**(48):11-18

[10] Chakraborty D, Chowdhary VM, Dutta D, Sharma JR. Classification of high spatial resolution image using multi circular local binary pattern and variance. International Journal of Electronics and Computer Engineering. 2013;**4**(6):1648-1653

[11] Weng Q. Remote sensing of impervious surfaces in the urban areas: Requirements, methods, and trends. Remote Sensing of Environment. 2012;**117**:34-49

[12] Chakraborty D, Sen GK, Hazra S. High-resolution satellite image segmentation using H¨older exponents. Journal of Earth System Science. 2009;**118**(5):609-617

[13] Mathivanan B, Selvarajan S. High spatial resolution remote sensing image segmentation using marker based watershed algorithm. Journal of Academia and Industrial Research. 2012;**1**(5):257-260

[14] Wang Z, Zhao S, Chen X. Watershed segmentation of high-resolution remotely sensed data. In: Proceedings of International Symposium on Remote Sensing & 20th Anniversary of the Korean Society of Remote Sensing; 2004. pp. 107-109

[15] Carleer AP, Debeir O, Wolff E. Assessment of very high spatial resolution satellite image segmentations. Photogrammetric Engineering and Remote Sensing. 2005;**71**(11):1285-1294

[16] Chakraborty D, Sen GK, Hazra S, Jeyaram A. Clustering for high resolution monochrome satellite image segmentation. International Journal of Geoinformatics. 2008;**4**(1):1-9

[17] Su T, Li H, Zhang S, Li Y. Image segmentation using mean shift for extracting croplands from high-resolution remote sensing imagery.

Remote Sensing Letters. 2015;**6**(12): 952-961

[18] Zhang X, Xiao P, Feng X, Wang J, Wang Z. Hybrid region merging method for segmentation of high-resolution remote sensing images. ISPRS Journal of Photogrammetry and Remote Sensing. 2014;**98**:19-28

[19] Chen B, Qiu F, Wu B, Du H. Image segmentation based on constrained spectral variance difference and edge penalty. Remote Sensing. 2015;**7**: 5980-6004

[20] Wang C, Shi AY, Wang X, Wu FM, Huang FC, Xu LZ. A novel multi-scale segmentation algorithm for high resolution remote sensing images based on wavelet transform and improved JSEG algorithm. Optik - International Journal for Light and Electron Optics. 2014;**125**(19):5588-5595

[21] Xia GS, Yang W, Delon J, Gousseau Y, Sun H, Maître H. Structural high-resolution satellite image indexing. In: ISPRS TC VII Symposium-100 Years ISPRS, Vol. 38; 2010. pp. 298-303

[22] Yang W, Yin X, Xia GS. Learning high-level features for satellite image classification with limited labeled samples. IEEE Transactions on Geoscience and Remote Sensing. 2015; **53**(8):4472-4482

[23] Huang X, Zhang L. An SVM ensemble approach combining spectral, structural, and semantic features for the classification of high-resolution remotely sensed imagery. IEEE Transactions on Geoscience and Remote Sensing. 2013;**51**(1):257-272

[24] Lucieer A, Stein A, Fisher P. Multivariate texture-based segmentation of remotely sensed imagery for extraction of objects and their uncertainty. International Journal of Remote Sensing. 2005;**26**(14): 2917-2936

[25] Malladi RK, Kasilingam D, Costa AH. Speckle filtering of SAR images using Hölder regularity analysis of the sparse code. In: IEEE International Geoscience and Remote Sensing Symposium; 2003. pp. 63998-64000

[26] Tahiri AM, Farssi SM, Touzani A. Textures in Images Classification Using a Multifractal Approach. IEEE SITIS. 2005. Available from: http://www.u-bourgogne.fr/SITIS/05/download/Proceedings/Files/f138.pdf

[27] Bourissou A, Pham K, Levy-Vehel J. A multifractal approach for terrain characterization and classification on SAR images. IGARSS. 1994;**3**:1609-1611

[28] Jain AK, Murty MN, Flynn PJ. Data clustering: A review. ACM Computing Surveys. 1999;**31**(3):264-323